Archives of Civil and Mechanical Engineering (2020) 20:121
https://doi.org/10.1007/s43452-020-00128-9

ORIGINAL ARTICLE

# Superplastic deformation of Mg–9Li–2Al–0.5Sc alloy after grain refinement by KoBo extrusion and cyclic forging

**Jan Dutkiewicz[1] · Damian Kalita[1] · Wojciech Maziarz[1] · Marek Faryna[1]**

Received: 13 March 2020 / Revised: 9 September 2020 / Accepted: 21 September 2020


**Abstract**
The quaternary Mg–9Li–2Al–0.5Sc alloy (in wt%) was prepared from pure components. After homogenization, the alloy was subjected to severe plastic deformation by KoBo extrusion and cyclic forging leading to grain refinement in the range of 0.5–2 μm of hexagonal close-packed (HCP) α phase. Deformed alloys showed high ultimate tensile strength near 200 MPa and good elongation in the range 30–40% at room temperature (RT). Large elongations close to 200% were obtained during the tensile test at a temperature of 200 °C. Deformed samples showed the presence of multiple voids confirming grain boundary sliding mechanism of deformation. Twins on $\{10\bar{1}2\}$ planes were identified using electron backscatter diffraction analysis, being in a good agreement with the earlier observation of Mg–Li and Mg–Sc alloys. Intermetallic phases such as cubic MgSc were identified in deformed alloys mostly within HCP α phase, whereas HCP $MgSc_2$ particles were observed within body-centered cubic (BCC) β phase. Intermetallic phases were responsible for RT strengthening of alloys and slightly lower tensile elongation during superplastic deformation. Formation of the HCP α phase was observed within the BCC β phase in tensile deformed alloys. Atomic-level nucleation of HCP phase within the β phase was identified by the use of high-resolution transmission electron microscopy technique.

**Keywords** Magnesium alloys · MgLiAlSc alloys · Superplastic deformation · KoBo extrusion · Cyclic forging · TEM

## 1 Introduction

Magnesium–lithium-based alloys are considered the lightest metallic engineering materials with a density of 1.35–1.65 g·cm$^{-3}$. They reveal high specific strength and stiffness [1]. The binary Mg–Li alloys with compositions near 8 wt% of Li consist of the hexagonal close packed (HCP) α and body-centered cubic (BCC) β phases and show very good plasticity and even superplastic properties at relatively low temperatures and moderate strain rates [2–5]. Their ductility is low in the as-cast state, intermediate when extruded and high after extrusion and ECAP (Equal Channel Angular Pressing) [2, 3]. The maximum superplastic deformation above 1000% was obtained in the temperature range of 200–300 °C at the deformation rate near $10^{-4}$ s$^{-1}$. The estimated grain size of the α and β phases after ECAP was in the range of 1–3 μm and the dominant deformation mechanisms in two-phase alloys was grain boundary sliding accommodated by slip controlled by the lattice diffusion [2, 3]. The lattice diffusion contributed to the grain growth mechanism during superplastic deformation [5]. At the low initial strain rates, the vacancies near grain boundaries had enough time to diffuse [4]. The concentration of vacancies formed cavitations, which turned into larger aggregates during the tensile test [4]. With the decrease of the initial strain rate both the amount and size of cavitations increased. There is only limited information on the role of the α and β phases during the deformation of Mg–Li based alloys, which possess different mechanical properties and often different grain sizes [6–12]. A small addition of other elements to binary Mg–Li alloys allows to improve the mechanical properties as well as helps to achieve strong

✉ Jan Dutkiewicz
dutkiewicz.j@imim.pl

Damian Kalita
d.kalita@imim.pl

Wojciech Maziarz
w.maziarz@imim.pl

Marek Faryna
m.faryna@imim.pl

[1] Institute of Metallurgy and Materials Science of the Polish Academy of Sciences, 25, Reymonta St., 30-059 Kraków, Poland

Published online: 06 October 2020

grain refinement during deformation processes [6]. The addition of 1% Al to the binary Mg–9Li alloy led to the grain refinement of both α and β phases in the range of 3–4 μm and very good superplastic properties after ECAP in the temperature range of 200–300 °C [7]. Low-temperature superplasticity was observed in the ternary Mg–10Li–1Zn alloy deformed at 150 °C. After tensile tests, the fine β precipitates were observed at grain boundaries due to dynamic recrystallization [8]. Also the (α + β) Mg–Li–(1–3) Zn alloys revealed the superplastic elongation at tensile deformation rate $10^{-2}$ $s^{-1}$, confirming the presence of grain boundary sliding in the alloys [9–12].

Some other additives, like Sn, improved mechanical properties of two-phase Mg–Li based alloys, attaining room temperature tensile strength near 320 MPa in the extruded Mg–8Li–1Al–0.5Sn alloy due to various fine precipitates containing tin [13]. Strontium added to the quaternary dual-phase Mg–Li–Al–Zn alloy resulted in high strength of the alloy with various intermetallic phases. Similarly, the additions of cerium and yttrium to the dual-phase Mg–Li–Zn alloys led to the formation of intermetallic phases precipitations and as result the development of high strength alloy with $\sigma_{0,2}$ = 256 MPa and improved hot working capability. Multidirectional forging caused the grain refinement below 3.75 μm (average size of α and β) and superplastic deformation up to 650% at the relatively high temperature of 350 °C in Mg–Li–Al–Zn–Sr alloy [14]. Fine equiaxed grains were observed in the extruded at 250 °C Mg–Li–Zn–RE alloy as a result of dynamic recrystallization [15]. Similar results were reported in [16] where the addition of 0.5 wt% of Y lead to strong grain refinement in the as-cast Mg–8Li–3Al–2Zn–0.5Y alloy with the optimum combination of tensile properties at an elongation of 16.9% at RT and ultimate tensile strength of 218.5 MPa. The addition of neodymium acted in a similar way and the improvement in mechanical properties was mainly attributed to grain refinement and dispersion strengthening by intermetallic phases such as AlLi, $MgLi_2Al$ and $Al_2Nd$ [17]. The ternary $MgLiAl_2$ phase coexisting with the α precipitates was observed in the super-light Mg–14Li–1Al alloy processed by conventional extrusion followed by ECAP pressing at room temperature. The β grains refinement up to 200 nm was observed after this process [18]. TCAP (Twist Chanel Angular Pressing) processing of dual-phase Mg–Li–Al alloys [19] showed the grain refinement of the α phase after 3 passes to 2.5 μm and along with the β phase down to 5 μm. This observation is contradictory to the other works, in which similar grain refinement of the α and β phases was observed after the ECAP [2, 3, 7]. However, the differences may result from the different grain measurement methods considering the subgrain formation [19]. Another very effective grain refinement method in Mg–Li based alloys is a multidirectional forging. The method is a very sensitive to deformation temperature and number of cycles, however, it allows to obtain extremely fine grains for both the α and β phases up to 300 nm as reported in [19]. Other Severe Plastic Deformation (SPD) method like High-Pressure Torsion (HPT) applied to the Mg–Li based alloy allowed to obtain particularly high superplastic deformation at relatively high strain rate as a result of high grain refinement down to 500 nm [21]. Furthermore, the applied shear during the HPT resulted in the dissolution of the metastable phases leading to single β phase formation after the process, as reported in [21]. Such a phenomenon was not observed when using other SPD methods, in which the formation of small HCP particles was observed within the β grains [18, 19].

There are a lot of discrepancies in the literature concerning the effect of various SPD methods on the α and β grains refinement, phase transitions during the deformation, mechanical properties as well as the influence of ternary and quaternary alloying elements on the deformation behavior. Therefore, in the present work the influence of small addition of Al and Sc to the dual-phase Mg–9Li alloy on the grain refinement using SPD methods, intermetallic phase formation and further superplastic deformation was studied in the newly developed Mg–9Li–2Al–0.5Sc alloy [22]. The effect of Sc addition to the Mg–Li based alloys on microstructure and mechanical properties was examined only in few papers showing that the small addition of Sc facilitate grain refinement up to the range of 1–2 μm [22] and increase the recrystallization temperature by more than 100 °C [24]. It was also proved, that small additions of Sc combined with other alloying elements, e.g. Al, caused strong age-hardening effect, which ensured optimal combination of strength and plasticity of the alloy [23, 25]. Furthermore, the effect of Sc addition on the superplastic deformation of MgLi base α + β alloys has not been investigated yet after severe plastic deformation [2–26]. The addition of scandium increases the ability of intermetallic phases formation, and therefore it improves the strength of two-phase Mg–Li alloys [18–26]. However, its effect on superplastic deformation ability was not yet investigated in spite of several studies on this subject already reported in the case of MgLi base alloys [2–12, 19, 20, 22]. Expected intermetallic phase formation should contribute to the strength increase and grain refinement being important factors in these ductile alloys of a very low density.

## 2 Experimental procedure

The quaternary Mg–9Li–2Al–0.5Sc (in wt%) alloy was prepared from pure Mg (99.99 wt%), Li (99.9 wt%), Al (99.99 wt%) and Sc (99.5 wt%). Because the alloy components differ significantly with respect to melting

temperature (Li 180.5 °C and Sc 1541 °C), the preparation of alloys was divided into two steps. First, the Mg–10Sc (wt%) based alloy was produced by induction melting. Subsequently, it was added to Li, Al and Mg in appropriate amounts leading to the desired Sc content in the final quaternary alloy. Because the liquid Li reacts immediately with graphite and many ceramics, the quaternary alloys were prepared in a molybdenum crucible. The alloy components were melted using high-frequency generator under a purified argon atmosphere and cast into a steel mold of the cylindrical shape of diameter 50 mm. The mass loss of such prepared alloys was below 0.5%. The castings were homogenized at 400 °C for 5 h. Then the alloy was extruded using KoBo facility to form bars of the rectangular shape of size 10 × 10 mm and length of a few meters, which corresponded to a reduction coefficient of $\lambda = 20$. The KoBo extrusion process applies the oscillating die during deformation. This ensures the cyclic changes of the deformation path in the material as a result of the change of the straining scheme. The method allows to perform the extrusion process without previous preheating of the material and up to higher strain rates than for conventional extrusion, even for hardly deformable materials like magnesium alloys or intermetallics. The KoBo process was described in more details in [27, 28]. The deformation was performed by extrusion with reversible rotations of the die at a frequency of 1 Hz and a radial range of 90°. It was manufactured at room temperature to avoid the dynamic grain growth assuming that scandium increases the recrystallization temperature and improves the grain refinement as observed in [24]. After the KoBo extrusion, the samples were deformed for a second time by multidirectional forging using Maxstrain Gleeble equipment. Cyclic forging was performed on the samples of a total length of 30 mm and forged length of 9 mm as shown in Fig. 1a, in two perpendicular directions at the temperatures of 150 °C and 200 °C. In each of compression cycle, the sample was deformed up to 50% (true strain 0.69) followed by compression in the perpendicular direction up to the same degree of deformation. Finally, 10 or 20 cycles were applied giving total true strains of 6.93 and 13.86, respectively. Figure 1a shows a photograph of the sample after such a process, whereas Fig. 1b presents stress/time graph registered during the multidirectional forging for the sample forged 20 times at 200 °C. The curves indicate that the compression stress required to the deformation of the material to 50% in height decrease with the number of cycles from 380 MPa to about 130 MPa. The negative sign of the stress is associated with the compression mode applied in the process. Tensile tests were performed on Shimadzu Autograph AG–X plus testing machine both at room temperature and at 200 °C. The constant strain rate of $10^{-4}$ $s^{-1}$ was applied in both cases. The strain was measured using a video-extensometer TRViewX system. The tensile samples were cut from multidirectionally forged materials to obtain specimens with cross section of 2.5 × 4.5 mm and gauge length 8.5 mm using Electrical Discharge Machine (EDM) to minimize undesired deformation effects. The tensile samples were cut in the extrusion direction (ED) as indicated in Fig. 1a. Microstructure and phase composition of the materials were studied by use of Transmission Electron Microscope (TEM) *Tecnai FEG G2 F20 S*uper twin equipped with EDAX microanalyzer as well as Scanning Electron Microscope (SEM) Philips XL30. Electron Backscatter Diffraction (EBSD) measurements were carried out on FEI Quanta 3D FEGSEM equipped with EBSD TSL system. For each of presented maps single dilatation clean up routine was applied (grain tolerance angle 5°, minimum grain size 5 pixels). Confidence index was 0.1 for all analysed maps. The analysed areas were 40 × 30 µm and the step size was 0.1 µm. For TEM observations thin samples from the material after SPD process and after tensile tests were cut by use of EDM, then dimpled and electropolished in an electrolyte consisting of 750 ml AR grade methanol, 150 ml butoxyethanol, 16.74 g magnesium

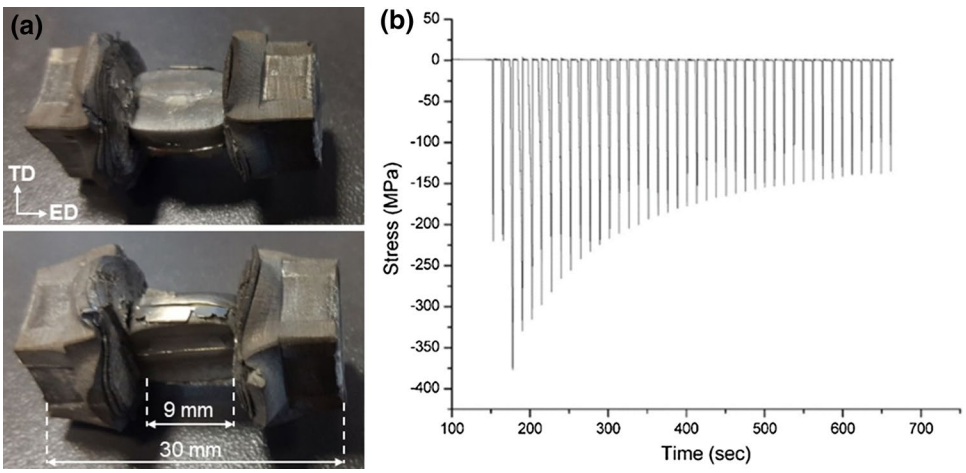


**Fig. 1** **a** Photograph of the specimen forged respectively in two perpendicular directions at 200 °C; **b** Stress vs time curves of specimen forged respectively 20 times in two perpendicular directions at 200 °C

perchlorate and 7.95 g lithium chloride, and finally, thinned using Leica EM RES101 ion beam thinner. The samples for the microstructural observations were prepared along the extrusion direction.

## 3 Results and discussion

Figure 2a shows the microstructure of the Mg–9Li–2Al–0.5Sc alloy initially cast and annealed at 400 °C. Figure 2b–d show backscattered electron (BSE) images taken from the samples after the KoBo extrusion followed by 10 and 20 forging cycles at 200 °C, respectively. The material in the initial state revealed a lamellar α (HCP) + β (BCC) microstructure, where the randomly oriented α phase grains are brighter, as marked in Fig. 2a. Microstructure of material after the KoBo extrusion revealed brighter areas of the α phase (depleted in Li) elongated in the extrusion direction. Between the α phase lamellae, darker areas enriched in Li, with visible grain boundaries of regular β phase are present. Fine, bright particles are located mainly within the β phase or at grain boundaries. The microstructure of the material is significantly refined after further 10 and 20 cycles of forging. It is worth to notice that precipitations of intermetallic phases (visible as very bright areas) were also refined with the increasing number of the cycles resulted in the increase of the frequency of their appearance. After 10 cycles of forging the precipitations form elongated bands parallel the extrusion direction of the bar while after 20 cycles they are uniformly distributed in the matrix.

Figure 3 shows RT tensile curves of the samples after the KoBo extrusion and after 10 and 20 forging cycles at 200 °C. Ultimate Tensile Strength (UTS) of the Mg–9Li–2Al–0.5Sc alloy after the KoBo extrusion reached the value of 160 MPa. Additional deformation by cyclic forging resulted in the increase of the strength of the material and the UTS at this stage exceeded the value of 200 MPa. All samples showed a good plasticity what indicates that the increase of strength is caused by grain refinement, not by defect density or high intermetallic phases density. TEM studies confirmed a very fine grain structure within the α phase after additional cycling. The

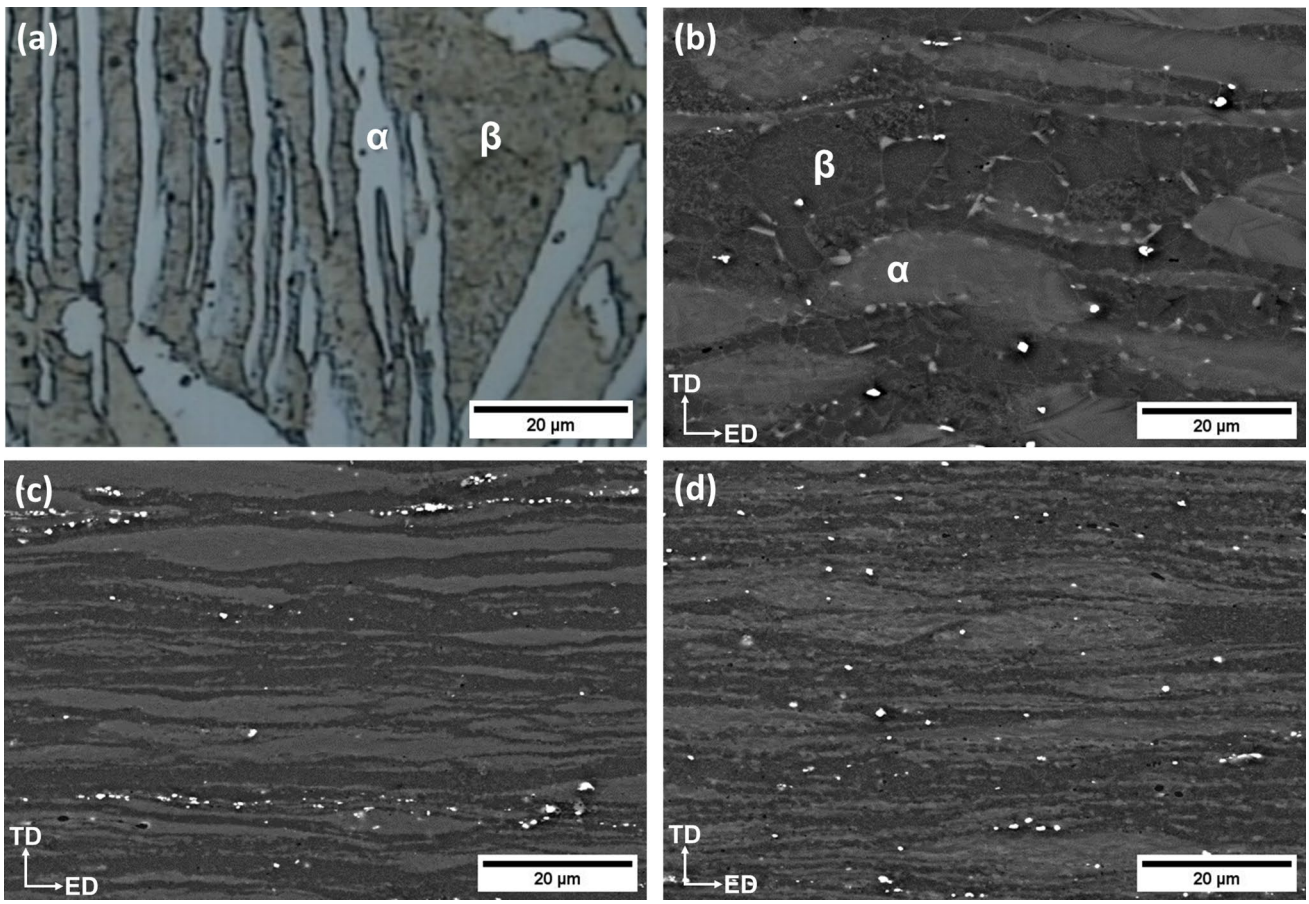


**Fig. 2** **a** Optical micrograph of the initial cast alloy annealed at 400 °C. **b–d** BSE micrographs of (**b**) sample deformed by the KoBo extrusion (**c**) after 10 forging cycles at 200 °C (**c**) and (**d**) after 20 forging cycles at 200 °C

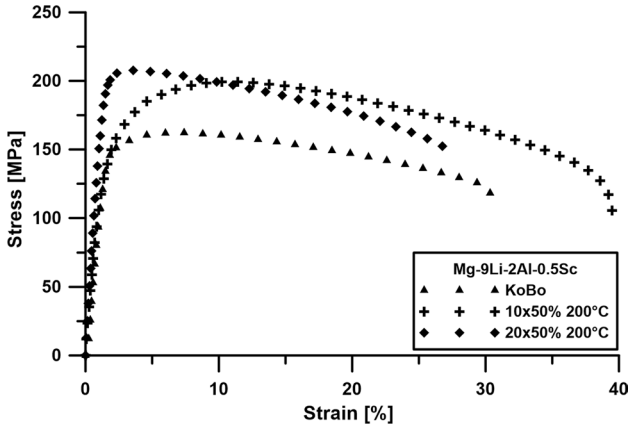


**Fig. 3** Tensile curves measured at RT of KoBo extruded sample and after following 10 and 20 forging cycles

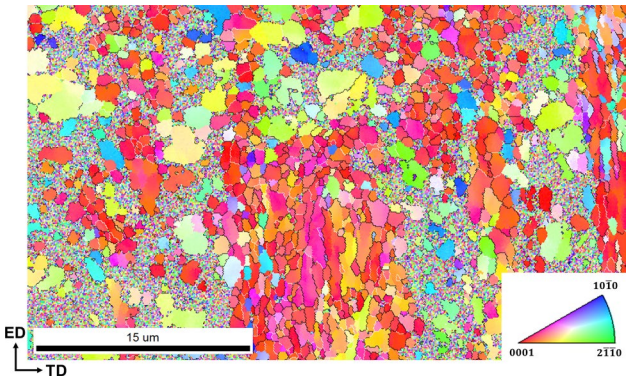


**Fig. 4** Inverse Pole Figure (IPF) map acquired for the HCP α-Mg phase of the sample after 20 forging cycles at 200 °C

further deformation by cyclic forging induced cracks within the material, leading to a decrease of plasticity for the sample forged 20 times. Mechanical properties of the investigated materials are higher than reported for dual-phase binary Mg–Li alloys, in which the strength after rolling approached the value of 120 MPa at similar elongation [29]. The dual-phase alloys containing Zn after the ECAP also showed a slightly lower strength (up to 180 MPa) but lower elongation [11, 30]. That was probably associated with the cracks formation after ECAP, similarly to our observations. Therefore, the samples for tensile tests were prepared from the regions away from forging tool edges. Only the β phase alloys with a high Al content (up to 5 wt%) attained a slightly higher strength, however, accompanied by a brittle behavior or high strength near 240 MPa and low plasticity below 3% [31]. Strengthening by intermetallic particles in these alloys was accompanied by a drastic drop of ductility.

In our previous work [22], we analyzed the texture formed during the KoBo extrusion of the Mg–9Li–2Al–0.5Sc alloy. The obtained results showed $\{0001\}<1010>$ preferred orientation of HCP α phase, while the texture of the bcc β phase was less developed were a weak texture $(111)[\bar{1}10]$ was observed. A similar type of texture of the α phase was observed in the extruded α phase Mg–Li alloys [32], in the rolled Mg–Li [29] and the Mg–Li–Al dual-phase alloys [33]. In the case of β phase, the observed texture was different comparing with literature, e.g. in [29] where the $\{001\}<110>$ texture of the rolled Mg–Li dual-phase alloys was identified. The differences may be caused either by a different deformation mode and or by ternary and quaternary additions.

Figure 4 shows the IPF map of the HCP α phase after 20 forging cycles at 200 °C. The β phase areas have not been analyzed, due to low quality of diffractions, which may be related to the heavier deformation of this phase during the forging as well as the formation of small precipitations of α phase as reported in [18, 19]. Grains within elongated α areas showed preferred orientation close to [0001], while the α grains pressed into the β phase during multiple slip resulted in more random orientations.

Figure 5a shows [0001] and $[10\bar{1}0]$ pole figures from the surface parallel to the extrusion direction from the KoBo extruded and cyclic forged sample measured by use of EBSD technique. One can see that there is a strong maximum of (0001) plane parallel to the extrusion direction. The maxima of $(10\bar{1}0)$ are distributed along extrusion direction, however, their directions are not as well defined as in the case of the basal plane. A similar type of texture with (0001) plane parallel to the rolling plane was observed in the rolled Mg–Li alloys [29], the rolled Mg–Li–Al dual phase alloy [33] and the rolled and annealed Mg–Sc alloy [34], however with the (0001) maxima more diffused toward the transverse direction. A graph in Fig. 5b shows the dependence of grain size versus area fraction in the KoBo extruded and cyclic forged sample. The highest amount of the HCP α grains have a size in the range of 0.5–2 μm and the calculated average grain size was $1.2 \pm 0.7$ μm. It is important to notice that fine grains of the α phase were also identified in the β phase areas, which suggests that during deformation the β phase is partially transformed into the α phase. Observed grains were finer and more homogeneous than that reported for the Mg–8Li–2Zn alloy [10], where the areas of fine grains of 1–2 μm diameter and also larger than 10 μm were observed after extrusion and rolling. Similarly, the larger grains were observed in the Mg–Li based alloys subjected to the ECAP, i.e. grains with size in the range of 1–7 μm was observed for the Mg–8Li deformed at 135 °C [3] or 5–10 μm in the case of Ti–8Li–1Zn processed at 200 °C [30].

In the Mg–9Li–1Zn alloy subjected to HRDSR (High-Speed Ratio Differential Speed Rolling) at 125 °C the grain size was refined down to 1–2 μm for both the α and β phases, although the literature suggested the presence of smaller

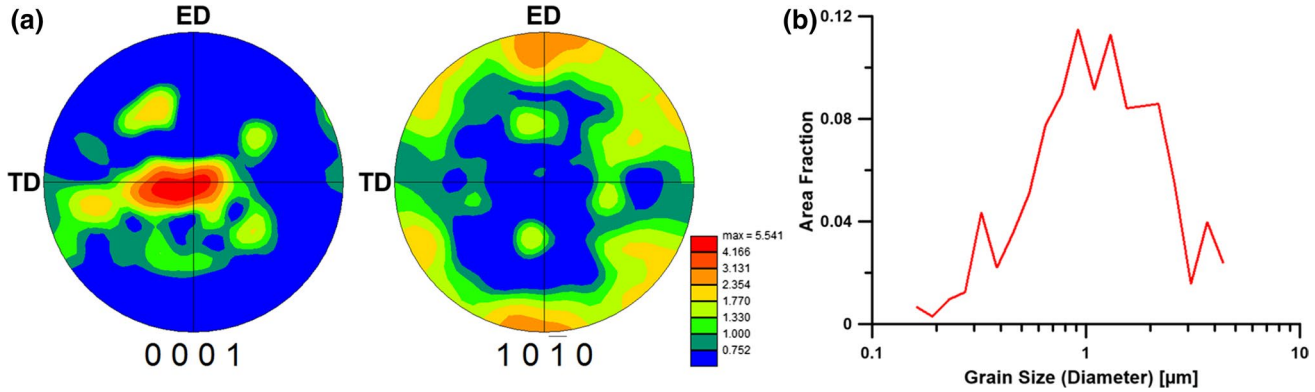


**Fig. 5** **a** 0001 and $10\bar{1}0$ pole figures, measured using EBSD technique, of the sample after KoBo extrusion and 20 cycles of forging at 200 °C; **b** graph showing area fraction—grain size dependence

subgrains revealed by TEM observation, where also fine α HCP particles were observed after SPD [12]. Other methods like HPT applied to the dual-phase Mg–Li alloys resulted in achieving the grain size in the range of 500 nm and leading to very good superplastic properties.

It is apparent that most of the SPD methods led to the grain refinement down to a few microns. In the case of ternary and quaternary alloys containing the alloying elements like Al or Zn, due to the hardening effect caused by intermetallic phases formation, the required deformation temperature is higher in comparison to binary Mg–Li alloys. The obtained results show that intermetallic particles observed in the investigated material have a pronounced impact on the stability of microstructure after the SPD process.

Figure 6 shows tensile curves for the KoBo extruded (a) and multidirectionally forged samples at 150 °C (b) and 200 °C (c). Tensile tests were performed at 200 °C at the strain rate of $10^{-4}$ $s^{-1}$. The image shown in Fig. 6c (see the insert) represents a typical initial sample and sample after the tensile test at 200 °C. In the case of KoBo extruded sample, the elongation at 200ºC reached the value of 42%, which is only slightly higher value in comparison to the sample tested at RT (Fig. 3). On the other hand, the considerable improvement of the plasticity was obtained in forged samples for which the elongations were in the range between 150 and 190%. This is associated with the significant grain refinement obtained by the combination of the KoBo extrusion process and the multidirectional forging. The obtained results are generally similar to those regarding superplastic deformation of the Mg–8Li–2Zn [10] and Mg–9Li–1Zn alloys [12] or, slightly lower than those, in the Mg–9Li–1Al alloy [7] at similar deformation range and temperature. However, elongation observed during superplastic deformation in the binary Mg–Li alloys were much higher, even at lower temperatures [2, 3, 20, 26], in comparison to the investigated quaternary Mg–Li–Al–Sc alloy, however, in most cases at higher deformation temperature of 300–400 °C. A probable reason for such an effect is the presence of intermetallic particles in the alloys contain ternary and quaternary additions, which are not observed in binary Mg–Li alloys. Moreover, the ternary and quaternary alloys are more interesting due to much higher room temperature strength as discussed above. The UTS is slightly lower for the alloy after cyclic forging at 150 °C (Fig. 6a), most probably due

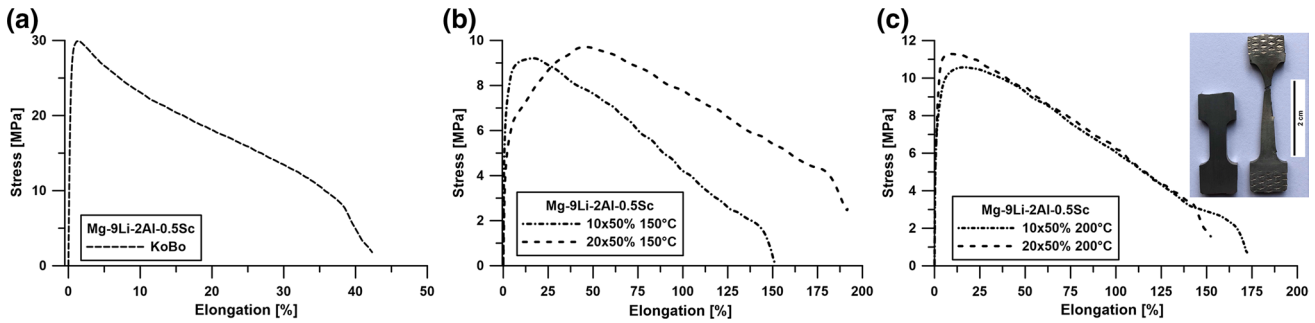


**Fig. 6** Tensile curves recorded at strain rate $10^{-4}$ $s^{-1}$ and temperature of 200 °C for the samples after KoBo **a** and after 10 and 20 cycles of forging at 150 °C **b** and 200 °C **c**. The insert presents the image of the sample before and after the tensile test performed at 200 °C

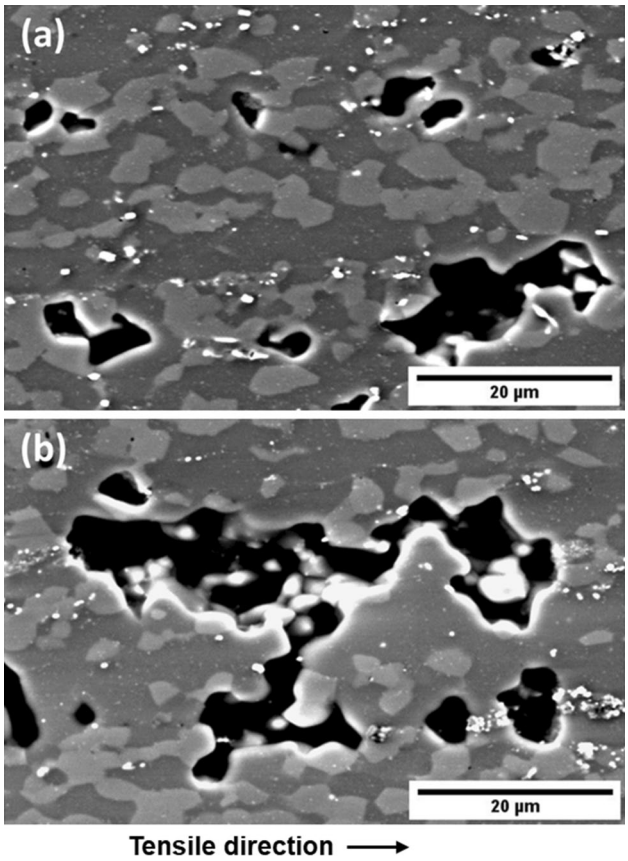


**Fig. 7** **a** BSE micrographs of tensile tested samples at 200 °C. KoBo extruded and cyclic forged **a** 20 times at 150 °C and **b** 20 times at 200 °C

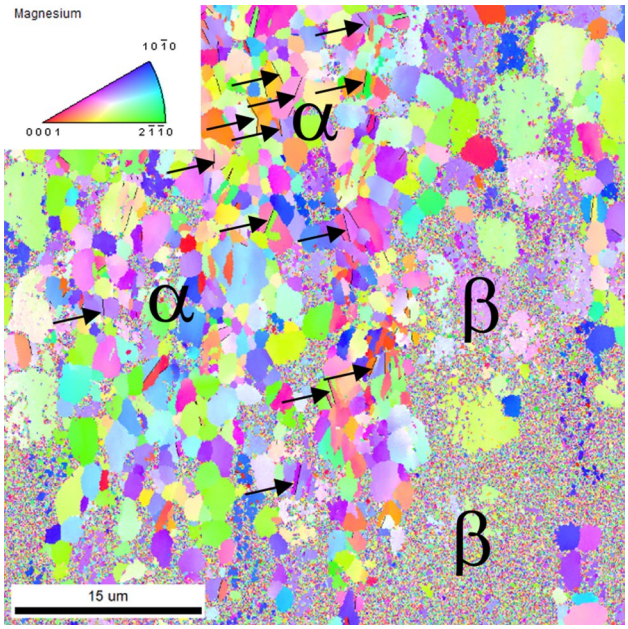


**Fig. 8** Inverse Pole Figure (IPF) of the HCP α-Mg phase from the area near fracture surface of tensile tested sample at 200 °C after deformation by cyclic forging 20 times at 200 °C; color-coded map of pole Fig. 0001 is shown as an insert

to slightly smaller grain size than in the case of the sample deformed at 200 °C, since grain boundary sliding is the main deformation mechanism in this case.

Figure 7a, b show the BSE images of microstructure after the tensile test, in which large voids of 5–10 µm in size can be seen. They are similar to those observed in the previous work on superplastic deformation in the Mg–Li based alloys [7]. Grains of both α and β phases grew after superplastic deformation. Before the fracture, there were many voids (visible as black areas in the microstructure), which were formed above all near the fracture region and the final fracture occurred most probably by the coalescence of those voids. The voids were formed frequently at the interface of α/β phase boundaries suggesting the participation of the boundaries in the slip process. Fine, bright intermetallic particles at the α/β interface were also spotted on the BSE images. Their contrast suggests that they are intermetallic particles enriched in heavier elements—Al and Sc in this case. The presence of intermetallic particles at the α/β interfaces is the barrier for slip and, therefore, obtained elongations in the present study and in [7, 10, 12] for the Mg–Li–Al and Mg–Li–Zn alloys were reported to be lower than for the binary Mg–Li alloys [2, 3, 20]. Therefore, the TEM/EDS analysis was performed to identify those phases as well as to study the nature of interface boundaries and defect densities.

To quantify the data regarding grain growth and texture changes during the superplastic deformation EBSD measurements were performed. Figure 8 shows IPF map from the area near the fracture surface of the sample forged 20 times at 200 °C before the tensile test at 200 °C. It can be clearly seen, that the grain size increased during the test, as compared to the samples after cyclic forging attaining the average size of $2.0 \pm 1.0$ µm. Finer grain area indicates the presence of β grains with fine α particles. Twins were not so far observed in the MgLi base alloys during superplastic deformation. However, in our study some $\{10\bar{1}2\}$ twins appeared within the α grains (as marked by black lines and arrows on the micrograph) in the heavily deformed area near necking, where the crystallographic slip predominated over grain boundary sliding mechanism. In other sites of the sample, no twins were observed. Twinning plane has been already identified in the magnesium alloys [35, 36] and in the Mg–Li–Al alloys as the $\{10\bar{1}1\}$ plane [18]. The presented IPF map does not show the orientation of the β phase grains due to difficulties associated with proper indexing of diffractions patterns from this phase. This may be related to higher defects density, since the softer BCC β phase underwent crystallographic slip deformation in addition to the grain boundary slip or partial transformation

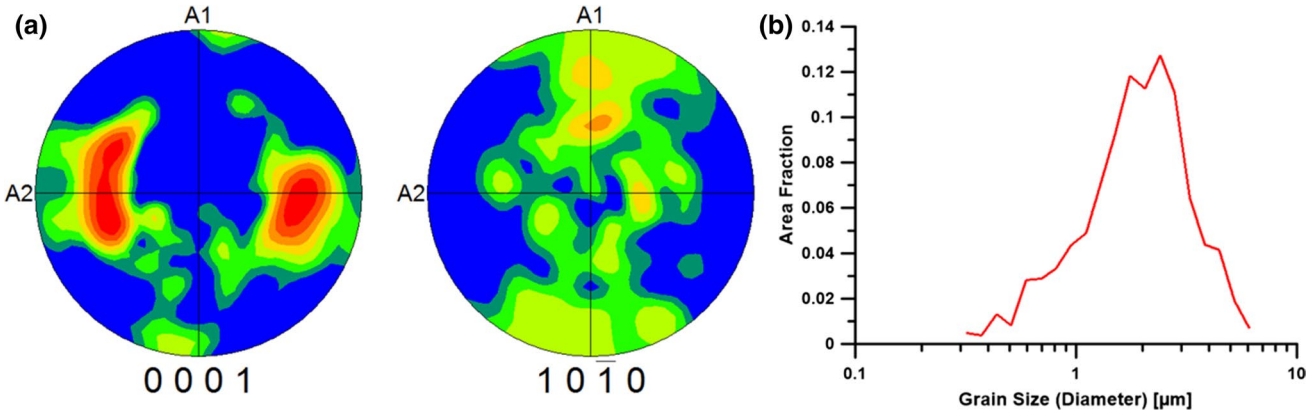


**Fig. 9** **a** 0001 and $10\bar{1}0$ pole figures calculated from EBSD measurements of HCP α grains of sample cyclic forged 20 times at 200 °C and tensile tested at 200 °C, **b** grain size distribution

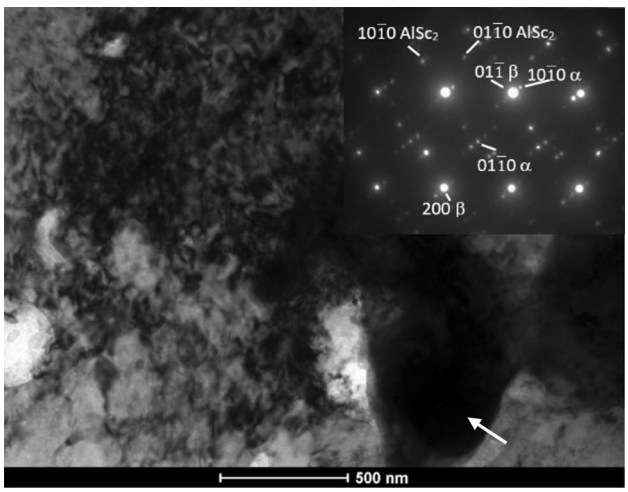


**Fig.10** TEM micrograph of BCC β grain of sample after 10 forging cycles at 200 °C and deformed during the tensile test up to fracture at 175% and SADP as insert with indexing showing [011] β + [0001] α and [0001] HCP $AlSc_2$

to the α phase during deformation. Fine-grained α phase areas appeared mostly within the areas where diffractions have not been properly indexed, i.e. within the BCC β grains. From the pole figures calculated from the individual grain orientations (Fig. 9a), the (0001) texture present after SPD changed due to rotation around direction parallel to the forging one indicating the participation of the crystallographic slip and grain boundary sliding within the α HCP phase. The highest population of grains was in the range of 2–3 μm (Fig. 9b) confirming their significant growth during superplastic deformation. As a result of superplastic deformation, the increased amount of the α-phase was observed in the fractured tensile samples. This can be attributed to the stress-induced transformation of the β phase to the α phase near the fracture region. Such a transformation was also noted in the literature [7, 18].

To identify the precipitates of other phases and confirm the results of the EBSD measurements regarding twins, grain size as well as to image crystal defects within the α and β grains, TEM studies of tensile tested samples were performed. Figure 10 shows a microstructure of the BCC β grain, where fine dark and bright particles can be seen within the grain together with a high density of dislocations. In the right bottom part of the micrograph a large, dark particle was identified that probably corresponds to fine, bright particles visible on the SEM images. From the selected area diffraction pattern (SADP) shown as an insert in Fig. 10, one can see that the [011] zone axis of the BCC β grain is perpendicular to the image plane. The $AlSc_2$ phase at [0001] zone axis orientation and the HCP α phase at the same zone axis orientation were also identified. The orientation relationship seems to be correct since densely packed {110} planes of the BCC β phase are parallel to {0001} plane of the HCP $AlSc_2$ and the HCP α phase. Electron diffraction confirmed earlier observations reported in [7, 18] that the α-phase formed after SPD due to stress and diffusion assisted phase transition, in which a portion of the β-phase is transformed into the HCP α one. The formation of $AlSc_2$ phase was not yet observed, however, the grain refining effect was reported in the Mg–Li–Sc alloys [37]. The precipitation of MgSc phase was reported in the ternary Mg–Li–Sc alloys [22], although no quaternary alloys have been investigated so far. Therefore, based on the BSE images and the results of SADP, it seems that the $AlSc_2$ phase can be considered to precipitate in the investigated alloys since many precipitations of intermetallic phases were found in the ternary Mg–Li–Al–X alloys [13–17].

Figure 11 shows a dark grain of the α phase surrounded by other α grains. Partially etched particles can be seen at the grain boundaries along with a high density of defects within

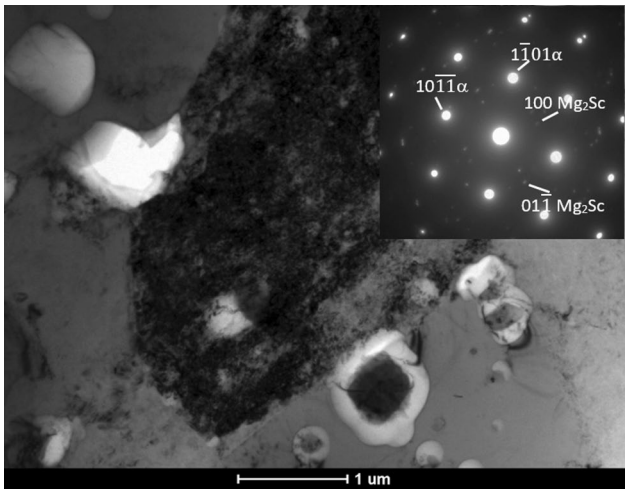


**Fig. 11** TEM microstructure of Mg–Li–Al–Sc alloy after 10 forging cycles at 200 °C and deformed during a tensile test at 200 °C up to fracture at 175% elongation and SADP shown as insert indexed as < 011 > zone axis of cubic $Mg_2Sc$ and [$12\bar{3}1$] Mg HCP α phase

the grains. SADP could be indexed as [$12\bar{3}1$] zone axis of the HCP α phase and [011] zone axis orientation of the cubic $Mg_2Sc$ phase. Relatively high dislocation density indicates the contribution of the crystallographic slip together with grain boundary slip to superplastic deformation of the sample. Such a statement supports also the observation concerning the change of the HCP α texture after the tensile deformation.

Figure 12 shows a section of the α/β phase boundary of the tensile tested sample up to fracture at 198% elongation at 200 °C after 20 cycles of forging. Intermetallic particles (marked by arrows) decorating grain boundary and a high density of crystal defects such as dislocations within the HCP α grains can be clearly seen. Such an observation confirms the significant deformation of the HCP α phase. From the SADP taken from the dark area of the central grain (shown in the up-right corner), the symmetrical [$01\bar{1}0$] HCP α zone axis orientation was identified. Weak reflections from the partially etched precipitates could be indexed according to [$02\bar{2}1$] zone axis orientations of the cubic MgSc phase.

Figure 13 shows HRTEM image taken of the alloy after 20 forging cycles at 150 °C and tensile tested at 200 °C up to elongation of 198%. A part of the grain is almost completely β → α transformed, as can be seen in the Fast Fourier Transformation (FFT) from the marked areas, where the corresponding orientations are either dominant the [111] β phase or the[$01\ \bar{1}\ 0$] α phase. In the lower part of the image, in addition to [111] BCC β, weak HCP α reflections can be observed, which indicate the nucleation of the α phase at the atomic scale without any distinct interface. Frequent defects indicate that the nucleation of the α phase occurred probably as regular stacking of densely packed planes. A poor contrast in some places in the HRTEM image from the lattice planes is probably due to the crystal defects such as dislocations. The majority of the area is already transformed into the HCP α phase showing the following crystallographic relationship: {111} β || {0001} α. This micrograph indicates that the transformation BCC → HCP takes place during superplastic tensile deformation at 200 °C as it has been also observed during SPD.

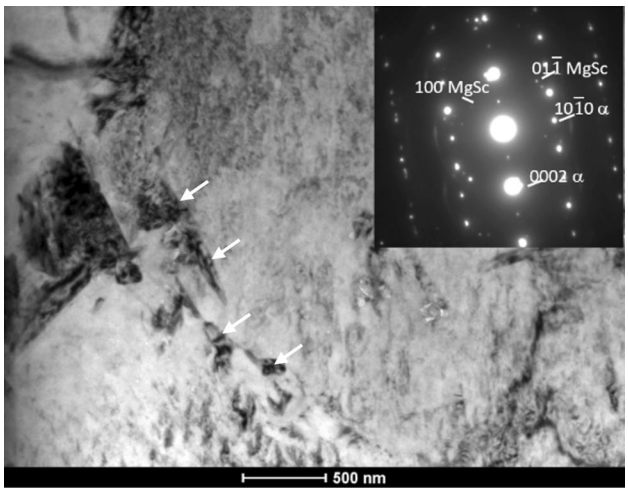


**Fig. 12** TEM microstructure of Mg–Li–Al–Sc after 20 forging cycles at 150 °C and deformed at 200 °C up to fracture at 198% elongation and SADP shown as insert indexed as < 01 1 0 > zone axis of Mg HCP α and [011] of cubic MgSc phase

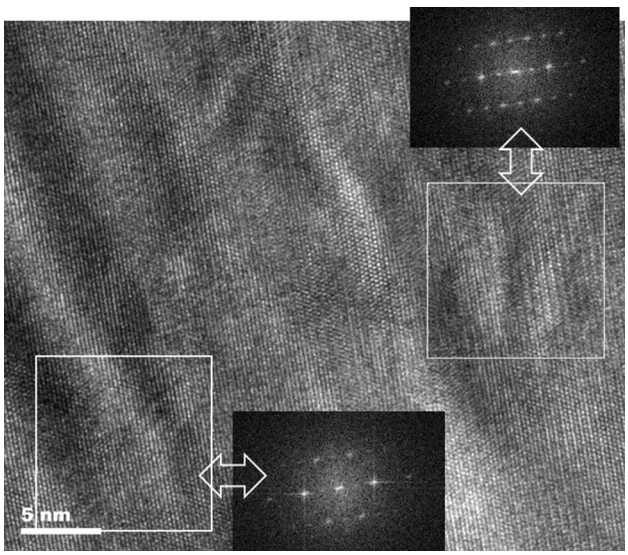


**Fig. 13** HRTEM of the investigated alloy after tensile test at 200 °C up to 198% of elongation. FFT from marked areas show [111] BCC β and [$01\ \bar{1}\ 0$] HCP α orientations

## 4 Conclusions

1. Significant grain refinement after KoBo extrusion and cyclic forging resulted in a fine grain material with the HCP α grain size in the range of 0.5–2 μm, which was nearly close to the finest grain in Mg–Li alloys obtained using HPT method. Deformed alloys showed high strength near 200 MPa UTS and good RT elongation near 40%.
2. Large elongations, similar to those reported for the Mg–Li–X alloys with intermetallic particles, were obtained in the investigated Mg–Li–Al–Sc alloys reaching elongations in the range of 150–200% at a temperature of 200 °C.
3. Superplastic deformation of the alloys after KoBo processing and cyclic forging showed frequent voids confirming grain boundary sliding mechanism. Texture of the HCP α phase after tensile deformation was different from the (0001) one after forging due to the rotation around the direction parallel to the forging direction, indicating the participation of crystallographic slip and grain boundary sliding within the α phase. Twins on $\{10\bar{1}2\}$ planes were identified by IPF map being in a good agreement with earlier observation of the Mg–Li and Mg–Sc alloys.
4. Intermetallic phases, such as cubic MgSc, were identified in deformed alloys, mostly within the α phase while HCP $AlSc_2$ and cubic $Mg_2Sc$ particles were discerned within the β phase. Intermetallic particles were responsible for RT strengthening of the alloys and slightly lower tensile elongation during superplastic deformation. Formation of the α phase was observed within the β phase in tensile deformed alloys. Atomic-level nucleation of the HCP phase within the β phase was possible to recognize by use of the HRTEM technique.

**Funding** The financial support of the National Science Center (NCN) under project number 2014/15/B/ST8/03184 is gratefully acknowledged.

**Data availability** The data that support the findings of this study are available from the corresponding author, upon reasonable request.

**Code availability** Not applicable.

### Compliance with ethical standards

**Conflict of interest** All authors declare that they have no conflict of interest.



## References

1. Wu RZ, Deng YS, Zhang ML. Microstructure and mechanical properties of Mg–5Li–3Al–2Zn–xRE alloys. J Mater Sci. 2009;44:4132–9.
2. Furui M, Xu C, Aida T, Inoue M, Anada H, Langdon TG. Improving the superplastic properties of a two-phase Mg–8% Li alloy through processing by ECAP. Mater Sci Eng A. 2005;410–411:439–42.
3. Furui M, Kitamura H, Anada H, Langdon TG. Influence of preliminary extrusion conditions on the superplastic properties of a magnesium alloy processed by ECAP. Acta Mater. 2007;55:1083–91.
4. Qu Z, Liu X, Wu R, Zhang M. The superplastic property of the as-extruded Mg–8Li alloy Mater. Sci Eng A. 2010;527:3284–7.
5. Cao FR, Ding H, Li YL, Zhou G, Cui JZ. Superplasticity, dynamic grain growth and deformation mechanism in ultra-light two-phase magnesium–lithium alloys. Mater Sci Eng A. 2010;527:2335–411.
6. Dong H, Xu S, Wang L, Kamado S, Wang L. Microstructures and mechanical properties of As–Cast and hot-rolled Mg–8.43Li–0.353Ymm (Y-riched mischmetch) alloy. Metall Mater Trans A. 2012;43:709–15.
7. Yang HP, Fu MW, To S, Wang GC. Investigation on the maximum strain rate sensitivity (m) superplastic deformation of Mg-Li based alloy. Mater Design. 2016;112:151–9.
8. Yoshida Y, Cisar L, Kamado S, Kojima Y. Low temperature superplasticity of ECAE processed Mg–10%Li–1%Zn Alloy. Mater Trans. 2002;43:2419–23.
9. Dong S, Imai T, Lim SW, Kanetake N, Saito N, Shigematsu I. Superplasticity in Mg–Li–Zn alloys processed by high ratio extrusion. Mater Manuf Process. 2008;23:336–41.
10. Liu X, Wu R, Niu Z, Zhang J, Zhang M. Superplasticity at elevated temperature of an Mg–8%Li–2%Zn alloy. J Alloys Compd. 2012;541:372–5.
11. Chang TC, Wang JY, Chu CL, Lee S. Mechanical properties and microstructures of various Mg–Li alloys. Mater Lett. 2006;60:3272–6.
12. Kim WJ, Kim MJ, Wang JY. Ultrafine-grained Mg–9Li–1Zn alloy sheets exhibiting low temperature superplasticity. Mater Sci Eng A. 2009;516:17–22.
13. Fu X, Yang Y, Hu J, Su J, Zhang X, Peng X. Microstructure and mechanical properties of as-cast and extruded Mg-8Li-1Al-0.5Sn alloy. Mater Sci Eng A. 2018;709:247–53.
14. Cao F, Xue G, Xu G. Superplasticity of a dual-phase-dominated Mg–Li–Al–Zn–Sr alloy processed by multidirectional forging and rolling. Mater Sci Eng A. 2017;704:360–74.
15. Chen Z, Li Z, Yu C. Hot deformation behavior of an extruded Mg–Li–Zn–RE alloy. Mater Sci Eng A. 2011;528:961–6.
16. Zhao J, Zhang J, Liu W, Wu G, Zhang L. Effect of Y content on microstructure and mechanical properties of as-cast Mg–8Li–3Al–2Zn alloy with duplex structure. Mater Sci Eng A. 2016;650:240–7.

17. Zhang J, Zhang Y, Wu G, Liu W, Zhang L, Ding W. Microstructure and mechanical properties of as-cast and extruded Mg–8Li–3Al–2Zn–0.5Nd alloy. Mater Sci Eng A. 2015;621:198–203.
18. Liu T, Wu SD, Li SX, Li PJ. Microstructure evolution of Mg–14% Li–1% Al alloy during the process of equal channel angular pressing. Mater Sci Eng A. 2007;460–461:499–503.
19. Dutkiewicz J, Bobrowski P, Rusz S, Hilser O, Tański TA, Borek W, Łagoda M, Ostachowski P, Pałka P, Boczkal G, Kuc D, Mikuszewski T. Effect of various SPD techniques on structure and superplastic deformation of two phase MgLiAl alloy. Met Mater Int. 2018;24:1077–89.
20. Matsunoshita H, Edalati K, Furui M, Horita Z. Ultrafine-grained magnesium–lithium alloy processed by high-pressure torsion: Low-temperature superplasticity and potential for hydroforming. Mater Sci Eng A. 2015;640:443–8.
21. Srinivasarao B, Zhilyaev AP, Gutiérrez-Urrutia I, Pérez-Prado MT. Stabilization of metastable phases in Mg–Li alloys by high-pressure torsion. Scripta Mater. 2013;68:583–6.
22. Dutkiewicz J, Kalita D, Maziarz W, Tański T, Borek W, Ostachowski P, Faryna M. Effect of KOBO extrusion and following cyclic forging on grain refinement of Mg–9Li–2Al–05Sc alloy. Met Mater Int. 2020;26:1004–14.
23. Dutkiewicz J, Rogal Ł, Kalita D, Fima P. Development of new age hardenable Mg-Li-Sc alloys. J Alloys Compd. 2019;754:686–96.
24. Sha G, Sun X, Liu T, Zhu Y, Yu T. Effects of Sc addition and annealing treatment on the microstructure and mechanical properties of the As-rolled Mg-3Li alloy. J Mater Sci Technol. 2011;27(8):753–8.
25. Wu H, Gao Z, Lin J, Chiu C. Effects of minor scandium addition on the properties of Mg–Li–Al–Zn alloy. J Alloys Compd. 2009;474:158–63.
26. Wu R, Yan Y, Wang G, Murr LE, Han W, Zhang Z, Zhang M. Recent progress in magnesium–lithium alloys. Int Mater Rev. 2015;60:65–100.
27. Korbel A, Bochniak W, Ostachowski P, Błaż L. Visco-plastic flow of metal in dynamic conditions of complex strain scheme. Metall Mater Trans A. 2011;42:2881–977.
28. Korbel A, Bochniak W. Stratified plastic flow in metals. Int J Mech Sci. 2017;128–129:269–76.
29. Zou Y, Zhang L, Wang H, Tong X, Zhang M, Zhang Z. Texture evolution and their effects on the mechanical properties of duplex Mg–Li alloy. J Alloys Compd. 2016;669:72–8.
30. Karami M, Mahmudi R. The microstructural, textural, and mechanical properties of extruded and equal channel angularly pressed Mg–Li–Zn alloys. Metall Mater Trans A. 2013;44:3934–46.
31. Park GH, Kim JT, Park HJ, Kim YS, Jeong HJ, Lee N, Seo Y, Suh JY, Son HT, Wang WM, Park JM, Kim KB. Development of lightweight MgLiAl alloys with high specific strength. J Alloys Compd. 2016;680:116–20.
32. Zeng Y, Jiang B, Yang QR, Quan GF, He JJ, Jiang ZT, Pan FS. Effect of Li content on microstructure, texture and mechanical behaviors of the as-extruded Mg-Li sheets. Mater Sci Eng A. 2017;700:59–655.
33. Kumar V, Govind R, Shekhar R, Balasubramaniam K, Balani K. Microstructure evolution and texture development in thermomechanically processed Mg–Li–Al based alloys. Mater Sci Eng A. 2012;547:38–50.
34. Kula A, Silva CJ, Niewczas M. Grain size effect on deformation behaviour of Mg–Sc alloys. J Alloys Compd. 2017;727:642–57.
35. Kumar MA, Beyerlein IJ, Lebensohn RA, Tome CN. Role of alloying elements on twin growth and twin transmission in magnesium alloys Mater. Sci Eng A. 2017;706:295–303.
36. Kim WJ, Han KH, Lee YJ, Kim H, Lee EK. First-principles studies on twinnability of magnesium alloys: effects of yttrium and lithium on (1011)[1012] compression twinning deformation. Met Mater Int. 2018;24:720–9.
37. Chiang CT, Lee S, Chu CL. Rolling route for refining grains of super light Mg–Li alloys containing Sc and Be. T Nonferr Met Soc. 2010;20:1374–9.